PHYSICAL REVIEW D **93,** 093018 (2016)

Tests of the triple Higgs boson form factor in $\mu^-\mu^+ \to HH$

G. J. Gounaris[1] and F. M. Renard[2]

[1]*Department of Theoretical Physics, Aristotle University of Thessaloniki, Gr-54124 Thessaloniki, Greece*
[2]*Laboratoire Univers et Particules de Montpellier, UMR 5299, Université Montpellier II, Place Eugène Bataillon CC072, F-34095 Montpellier Cedex 5, France*

(Received 15 October 2015; published 27 May 2016)

We study the sensitivity of the process $\mu^-\mu^+ \to HH$ to the q^2 dependence of the HHH form factor, which can reflect the Higgs boson structure, especially in the case of compositeness. We compute the Born and one-loop SM contribution to this process. We then show how the $\mu^-\mu^+ \to HH$ polarized and unpolarized cross sections are modified by the presence of various types of anomalous contributions to the HHH form factor, in particular Higgs constituents in the case of compositeness.

DOI: 10.1103/PhysRevD.93.093018

I. INTRODUCTION

In spite of the discovery [1] of the Higgs boson [2], as expected in the standard model (SM) [3], the SM cannot be the last word, and physics beyond the SM (BSM) should exist [4]. A review on Higgs physics is, for example, made in Ref. [5]. With respect to BSM, various types of proposals have been made, leading, for example, to anomalous Higgs boson couplings [6,7] or to couplings of the Higgs boson to new visible or invisible particles [8], particularly in the case of Higgs boson compositeness [9–13].

There are many processes (involving Higgs boson production or decay) in which such Higgs boson couplings, differing from SM predictions, could be observed. However, in most of them, the Higgs boson is on shell, and such a departure could not obviously tell whether it is caused by Higgs compositeness. This is particularly the case if the Higgs boson is coupled to an invisible sector.

The observation of a suitable Higgs boson form factor, though, could give an answer to such questions. Indeed, a composite particle (like the proton or the pion) should have a form factor. But contrarily to the case of the proton and the pion, we do not have a γHH or a ZHH vertex for studying the H form factor.

In this paper, we concentrate on the HHH form factor, that is, at a $q^2 \equiv s$ dependence of the HHH vertex when one H, with momentum q, is off shell. The scale of this dependence could be in the TeV range; see, e.g., Ref. [9].

There are various processes which involve the HHH coupling, but not necessarily the form factor with one H far off shell, in which we are interested. Such processes at the LHC are $gg \to H \to HH$ (with g denoting a gluon) or $ZZ \to H \to HH$, $W^+W^- \to H \to HH$ [14], but these require complex theoretical and experimental analyses, before reaching the structure of the HHH coupling. Similarly, the $\gamma\gamma \to H \to HH$ process also involves a complex initial one-loop H coupling related to the HHH form factor.

The simplest process directly sensitive to an HHH form factor effect is then probably $\mu^-\mu^+ \to HH$, observable at a future $\mu^-\mu^+$ collider [15]. Even if this will be realizable only in the far future and under the condition of the obtention of a very high luminosity, this process is particularly interesting because in nonstandard Higgs models the $H\mu\mu$ coupling may still be similar to the SM one, whereas the Higgs boson self-coupling and the Higgs boson couplings to heavy fermions may be very different; see, e.g., Ref. [11].

So, below, we analyze $\mu^-\mu^+ \to HH$ in this spirit. We start by computing the SM Born and one-loop contributions to the helicity amplitudes and cross sections. At Born level, they are due to s-channel H exchange and (at a weaker level) to t- and u-channel μ exchange. At one-loop level, the corrections involve various triangles, boxes, and μ and H self-energy bubbles. Some of these terms (the "right triangles" and the "bubbles with four-leg couplings and H self-energy diagrams") already create contributions to the HHH form factor from the usual scalars, fermions, and gauge boson loops, but they are relatively small, at order α. We collect them in the Appendix, and we illustrate their corresponding (modest) s dependence.

We then compute examples of new contributions which could be induced either by Higgs boson compositeness or by the couplings of the Higgs boson to a new set of particles. Illustrations show how such contributions can generate spectacular differences in the s dependence of the HHH form factor, with respect to the one predicted by the SM.

These different one-loop corrections reflect in the various amplitudes and cross sections and could be useful for guessing what type of contribution is necessary in order to explain a possible departure of the measurements with respect to the SM expectation. We separately consider the helicity-conserving (HC) and the helicity-violating (HV) amplitudes and the polarized cross sections, as these ones may be measurable in this process [16].

Section II is devoted to the presentation of the SM Born amplitudes and cross sections of the $\mu^-\mu^+ \to HH$ process, and Sec. III is devoted to the SM one-loop contributions.

Examples of anomalous HHH contributions effects are described in Sec. IV. In the concluding Sec. V, we summarize our results, and we mention that this type of study of the effect of the HHH form factor could also be done in several other (but more complex) HH production processes.

II. SM BORN AMPLITUDES AND CROSS SECTIONS

The SM Born amplitude of the $\mu^-\mu^+ \to HH$ process is due to three diagrams: the s-channel H exchange with an initial $(\mu^-\mu^+H)$ and a final (HHH) coupling as well as two diagrams with t- and u-channel $\mu^\mp$ exchange with up and down $(\mu^-\mu^+H)$ couplings. The invariant Born amplitude is

$$A^{\rm Born}(\mu^-\mu^+ \to HH) = -\frac{e^2 g_{\mu\mu H} g_{HHH}}{s - m_H^2 + i m_H \Gamma_H}\, \bar{v}(l',\lambda') u(l,\lambda) - e^2 g_{\mu\mu H}^2 \left[\frac{\bar{v}(l',\lambda')(\not{q}' + m_\mu) u(l,\lambda)}{t - m_\mu^2} + \frac{\bar{v}(l',\lambda')(\not{q}'' + m_\mu) u(l,\lambda)}{u - m_\mu^2}\right], \quad (1)$$

where (λ,λ') are the (μ^-,μ^+) helicities, (l,l',p,p') are the (μ^-,μ^+,H,H) momenta, and we also define

$$q = l + l', \quad q' = l - p = p' - l', \quad q'' = l - p' = p - l', \quad s = q^2, \quad t = q'^2, \quad u = q''^2 \quad (2)$$

and the couplings

$$g_{\mu\mu H} = -\frac{m_\mu}{2 s_W m_W} = -\frac{m_\mu}{e v}, \qquad g_{HHH} = -\frac{3 m_H^2}{2 s_W m_W} = -\frac{3 m_H^2}{e v}, \quad (3)$$

where the final HH are symmetrized.

The corresponding Born helicity amplitudes are

$$F^{\rm Born}_{\lambda,\lambda'}(s,\theta) = \frac{e^2 g_{\mu\mu H} g_{HHH}}{s - m_H^2 + i m_H \Gamma_H} \sqrt{s}\, \delta_{\lambda,\lambda'} + e^2 g_{\mu\mu H}^2 \left[\frac{1}{t - m_\mu^2} - \frac{1}{u - m_\mu^2}\right] (2\lambda) p_H \sqrt{s} \sin\theta\, \delta_{\lambda,-\lambda'}, \quad (4)$$

where $p_H = \sqrt{s/4 - m_H^2}$ and θ is the c.m. scattering angle between l and p. Note that we computed them from the invariant amplitude in Eq. (1) by neglecting the $m_\mu/\sqrt{s}$ terms appearing in the μ propagator and in the precise expressions of the Dirac spinors. These Born amplitudes are already factorized by one or two $g_{\mu\mu H}$ couplings proportional to m_μ/m_W so that there is no need for keeping these negligible corrections.

Note also that s-channel part in Eq. (4) is angle independent and purely HV, due to the $\delta_{\lambda,\lambda'}$ term, which violates the high-energy helicity conservation rule $\sum \lambda_{\rm in} = \sum \lambda_{f\rm in}$ [17]. This term dominates at low energy, but it decreases like $1/\sqrt{s}$ as the energy increases.

The t- and u-channel parts are purely HC, when neglecting $m_\mu/\sqrt{s}$ terms. They tend to a constant at high energy and are forward-backward antisymmetric (vanishing at $\pi/2$). They are about 100 times weaker than the s-channel part, though, because of their additional small $g_{\mu\mu H}$ coupling factor.

So, finally the only non-negligible Born amplitudes are the HV ones (i.e., those due to the s-channel H exchange) in which we are interested, because of their proportionality to the HHH coupling. This is the first remarkable feature of the $\mu^-\mu^+ \to HH$ process.

The cross section for unpolarized $\mu^\mp$ beams is

$$\frac{d\sigma}{d\cos\theta} = \frac{p_H}{64\pi s\sqrt{s}} \sum_{\lambda,\lambda'} |F_{\lambda,\lambda'}(s,\theta)|^2. \quad (5)$$

Cross sections with left-handed or right-handed polarized $\mu^\mp$ beams will also be considered. Note that, due to the final HH symmetrization, the cross sections are necessarily forward-backward symmetric.

III. SM ONE-LOOP CONTRIBUTIONS

The one-loop corrections to the above Born terms contain various types of diagrams; triangle diagrams for initial and final vertices and H self-energy bubbles for s-channel H exchange; triangle diagrams for up or down vertices and $\mu^\mp$ self-energy bubble for t, u-channel $\mu^\mp$ exchange; and several types (direct, crossed, and twisted) of box diagrams. Some of the triangles and bubbles are divergent, and a choice of renormalization scheme has to be made, consisting in the addition of specific counterterms canceling these divergences. There are various schemes for this, which differ by their choice of experimental inputs; see Ref. [18]. One may, for example, use the on-shell (OS) scheme; a special application to SM and minimal supersymmetric SM Higgs couplings is done in Ref. [19].

However, in the present study, we are essentially interested in the s dependence of the HHH vertex (to be then compared with possible new physics effects) and not in its precise renormalized on-shell value, which will be difficult to measure accurately anyway. For this purpose, we will compute the various one-loop terms in the super-simple renormalization scheme (SRS) scheme [20] which give simple high-energy expressions, the contents of which are immediately readable and instructive, in particular for suggesting possible models for new contributions.

We next list the various diagrams and their relative importance:

(1) In the s-channel sector, we find:

(a) left triangles:

$$(W\nu W),(Z\mu Z),(\mu Z\mu),(G\nu G),(G^0\mu G^0),$$
$$(H\mu H),(\mu G^0\mu),(\mu H\mu),$$

followed by s-channel H exchange and a final HHH coupling.

(b) left triangles connected to the final HH by a four-leg coupling:

$$(W\nu W)+(WWHH),\quad (Z\mu Z)+(ZZHH),$$
$$(G\nu G)+(GGHH),$$
$$(G^0\mu G^0)+(G^0G^0HH),\quad (H\mu H)+(HHHH).$$

Denoting by $T^{\rm SM}_{\rm left}$ the sum of the a and b diagrams, the implied helicity amplitude is written as

$$F^{\rm left\,SM}_{\lambda,\lambda'}=\frac{eT^{\rm SM}_{\rm left}(s)g_{HHH}}{s-m_H^2+im_H\Gamma_H}\sqrt{s}\delta_{\lambda,\lambda'},\quad (6)$$

which is HV, like the s-channel Born terms, but is numerically small (100 to 1000 times smaller than Born, as expected from the α factor occurring for a one-loop correction without special enhancement effect).

(c) H self-energy and right triangles:

The implied amplitude consists of two parts. The first part $T_{\rm se}({\rm SM})$ involves an initial $(\mu\mu H)$ coupling followed by H self-energy bubbles and a final g_{HHH} coupling. The second part, $T_{\rm tri}({\rm SM})$, involves an initial $(\mu\mu H)$ coupling followed by H s-channel exchange and either a SM HHH form factor or a bubble and a four-leg coupling to HH. The sum of these two parts,

$$T^{\rm SM}_{HHH}(s)=T_{\rm se}({\rm SM})+T_{\rm tri}({\rm SM}),\quad (7)$$

leads to the helicity amplitude

$$F^{HHH\,{\rm SM}}_{\lambda,\lambda'}=\frac{eg_{\mu\mu H}T^{\rm SM}_{HHH}(s)}{s-m_H^2+im_H\Gamma_H}\sqrt{s}\delta_{\lambda,\lambda'},\quad (8)$$

which, as Eq. (6), is also HV and angle independent. The long list of contributions to $T^{\rm SM}_{HHH}$ is collected in the Appendix. It is found that, above the tt threshold, it is largely dominated by the ttt contribution. Numerically, the amplitude in Eq. (8) contains important real and imaginary parts, comparable to the HV Born terms in[1] Eq. (4).

[1]Note that the SRS scheme [20] is globally satisfactory above ~1 TeV.

(2) In the t, u sectors, we find:

(a) up or down triangles with $\mu^\mp$ exchange:

$$(\nu WW),(\mu ZZ),(\mu HH),(\nu GG),(\mu G^0G^0),$$
$$(Z\mu\mu),(H\mu\mu),(G^0\mu\mu).$$

Among them, non-negligible contributions only come from the (νWW) and (μZZ) triangles, which produce HV contributions (still 100 times weaker than the Born ones) and tending to an angular symmetric constant at high energy. The other terms lead essentially to small HC amplitudes, like the corresponding Born ones in Eq. (4).

(b) $\mu^\mp$ self-energy bubbles:

These t-and u-channel μ exchanges, which were already small at the Born level, lead to very small HC contributions when μ self-energy bubbles are added.

(3) Boxes are of two types: the direct boxes

$$(\nu WWW),(\mu ZZZ),(\nu GGG),(\mu G^0G^0G^0),$$
$$(\mu HHH),(Z\mu\mu\mu),(H\mu\mu\mu),(G^0\mu\mu\mu)$$

and the corresponding crossed ones and the twisted boxes

$$(Z\mu\mu Z),(H\mu\mu H),(G^0\mu\mu G^0)$$

and the corresponding crossed ones. Among them, the important contributions come from (νWWW), (μZZZ), and their crossed boxes because of the presence of W, Z couplings and the total absence of suppressed $H\mu\mu$ couplings. The induced invariant amplitudes are then given by

$$\begin{aligned}A_{\nu WWW}&=-2\alpha^2g^2_{WWH}g^2_{W\mu L}\\&\quad\times\{-m_\mu D_{11}I_{1L}+I_{1pL}(D_{12}-D_{13})\},\\A_{\mu ZZZ}&=\alpha^2g^2_{ZZH}\{4m_\mu g_{Z\mu L}g_{Z\mu R}I_1D_0\\&\quad-2[-m_\mu D_{11}(g^2_{Z\mu L}I_{1L}+g^2_{Z\mu R}I_{1R})\\&\quad+(g^2_{Z\mu L}I_{1pL}+g^2_{Z\mu R}I_{1pR})(D_{12}-D_{13})]\},\end{aligned}\quad (9)$$

written in terms of Passarino-Veltman D functions [21], and the helicity forms decomposed as

$$\begin{aligned}I_1&=\bar v(l',\lambda')P_Lu(l,\lambda)\to-\sqrt{s}\delta_{\lambda,\lambda'},\\I_{1L}&=\bar v(l',\lambda')P_Lu(l,\lambda)\to-\sqrt{s}\delta_{\lambda,\lambda'}\delta_{\lambda,-},\\I_{1R}&=\bar v(l',\lambda')P_Ru(l,\lambda)\to-\sqrt{s}\delta_{\lambda,\lambda'}\delta_{\lambda,+}\end{aligned}\quad (10)$$

for the HV contributions which are suppressed by m_μ factors, and

$$
\begin{aligned}
I_{1p} &= \bar{v}(l',\lambda')\not{p}u(l,\lambda) \\
&\to -p_H\sqrt{s}\sin\theta\delta_{\lambda,-\lambda'}(\delta_{\lambda,-}-\delta_{\lambda,+}), \\
I_{1pL} &= \bar{v}(l',\lambda')\not{p}P_L u(l,\lambda) \\
&\to -p_H\sqrt{s}\sin\theta\delta_{\lambda,-\lambda'}\delta_{\lambda,-}, \\
I_{1pR} &= \bar{v}(l',\lambda')\not{p}P_R u(l,\lambda) \\
&\to p_H\sqrt{s}\sin\theta\delta_{\lambda,-\lambda'}\delta_{\lambda,+},
\end{aligned} \tag{11}
$$

for the HC contributions. In Eq. (9), the couplings

$$
g_{W\mu L}=\frac{1}{s_W\sqrt{2}},\quad g_{Z\mu L}=-\frac{1-2s_W^2}{2s_Wc_W},\quad g_{Z\mu R}=\frac{s_W}{c_W},
$$
$$
g_{WWH}=\frac{m_W}{s_W},\quad g_{ZZH}=\frac{m_Z}{s_Wc_W} \tag{12}
$$

are used. Notice that the HC amplitudes of these boxes do not involve any mass suppressed coupling constant, such that they are only reduced by the one-loop α/π factor. For comparison, the Born HC amplitudes (due to t- and u-channel $\mu^{\mp}$ exchange) are reduced by the factor $(m_\mu/m_W)^2$. Because of these features, the box HC amplitudes are $(\frac{\alpha}{\pi})(\frac{m_W}{m_\mu})^2\sim 1000$ times larger then the HC Born ones and have a size almost comparable to the Born HV amplitudes. Both real and imaginary parts are important.

The remaining box HV contributions coming from m_μ terms do not have this enhancement and get the usual α/π reduction factor as compared to the Born terms.

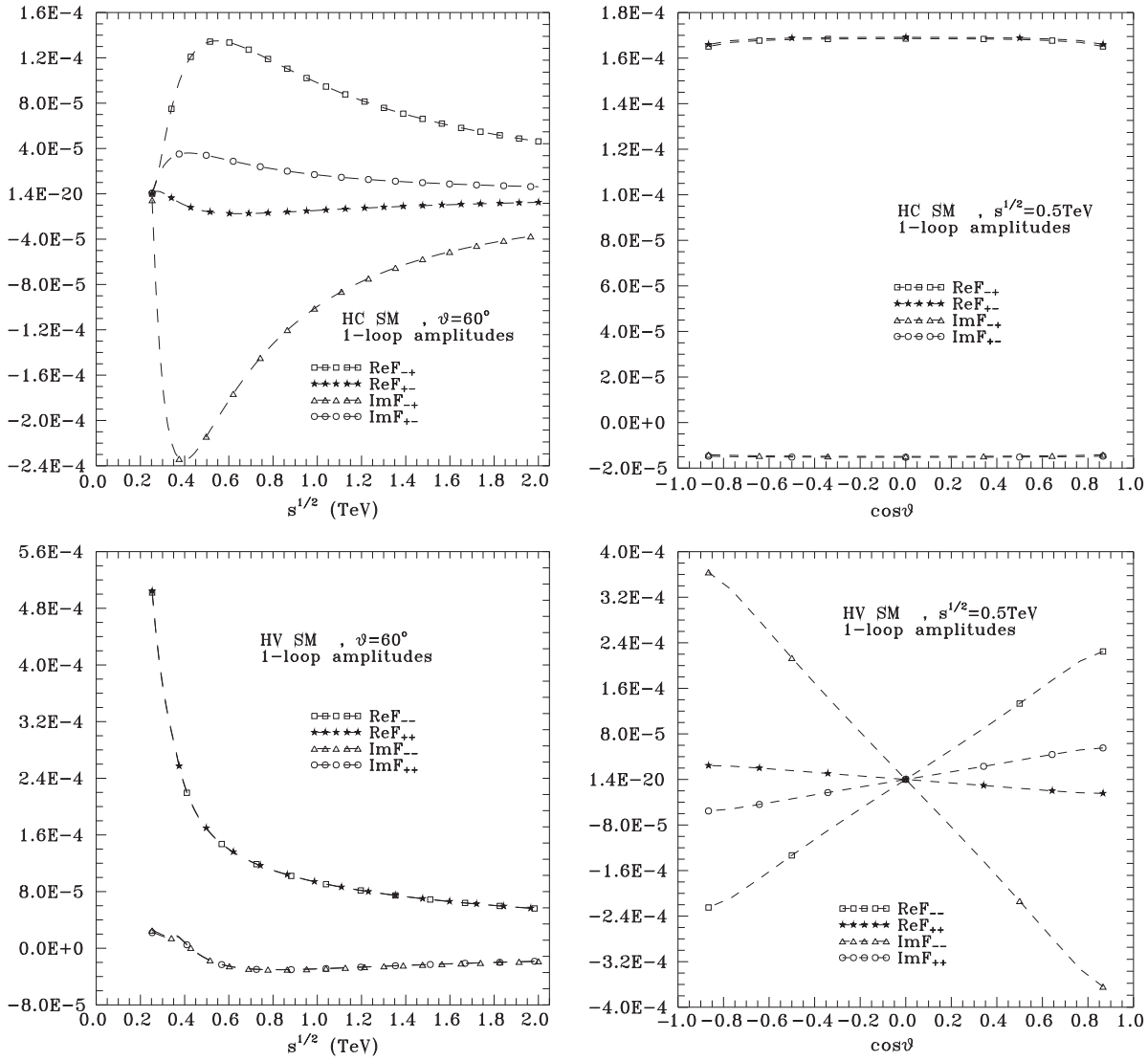

FIG. 1. The complete SM one-loop HC amplitudes (upper panels) and the corresponding HV amplitudes (lower panels). Left panels present the energy dependencies at $\theta=60°$, while right panels present the angular dependencies at $\sqrt{s}=0.5$ TeV.

A. Resulting total SM amplitudes and cross sections

These are constructed by summing the various one-loop contributions and adding them to the Born ones. The important terms are the HV Born term of Eq. (4), the H self-energy and HHH right triangles of Eq. (8) coming essentially from top-quark diagrams (see the Appendix), and the aforementioned contribution from the two boxes leading to Eq. (9).

These final complete one-loop results (Born + one-loop diagrams) for the HC and HV SM helicity amplitudes are illustrated in Fig. 1, where we show their energy and angle dependencies. Note that these complete SM, HC, and HV amplitudes have comparable sizes, although their s and θ dependencies are rather different. In particular, the two HC amplitudes almost coincide at 0.5 TeV (upper right panel), which also happens for the HV amplitudes at $\theta = 60°$, in a wide range of energies (lower left panel).

The corresponding (complete one-loop) cross sections, shown in Fig. 2, reflect the properties of the unpolarized cross sections defined in Eq. (5) and the $\mu^{\mp}$ polarized cross sections denoted as $d\sigma_{\lambda\lambda'}/d\cos\theta$. For the latter, the alternative notation indicating whether the contributing amplitudes are HV or HC may also be inspiring:

$$d\sigma_{LL} \equiv d\sigma_L(HV), \qquad d\sigma_{RR} \equiv d\sigma_R(HV),$$
$$d\sigma(HV) \equiv d\sigma_L(HV) + d\sigma_R(HV), \tag{13}$$

$$d\sigma_{LR} \equiv d\sigma_L(HC), \qquad d\sigma_{RL} \equiv d\sigma_R(HC),$$
$$d\sigma(HC) \equiv d\sigma_L(HC) + d\sigma_R(HC). \tag{14}$$

As seen in Fig. 2, the HV differential cross sections are angularly constant at $\sqrt{s} = 0.5$ TeV and reflect mainly the s-channel H exchange parts containing the effect of the

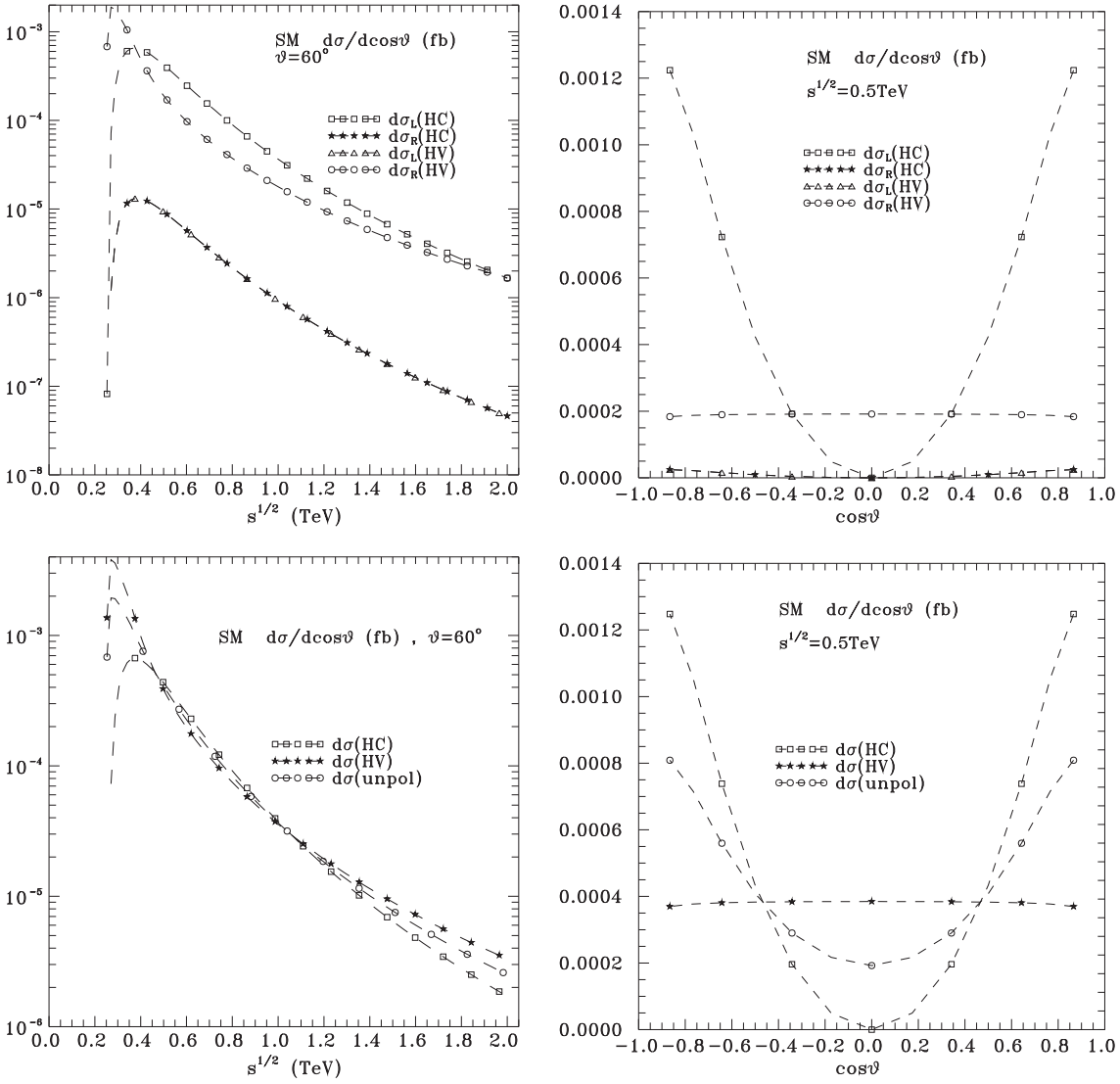

FIG. 2. SM one-loop differential cross sections as defined in Eqs. (13), (14). Left panels present the energy dependencies at $\theta = 60°$, while right panels present the angular ones at $\sqrt{s} = 0.5$ TeV.

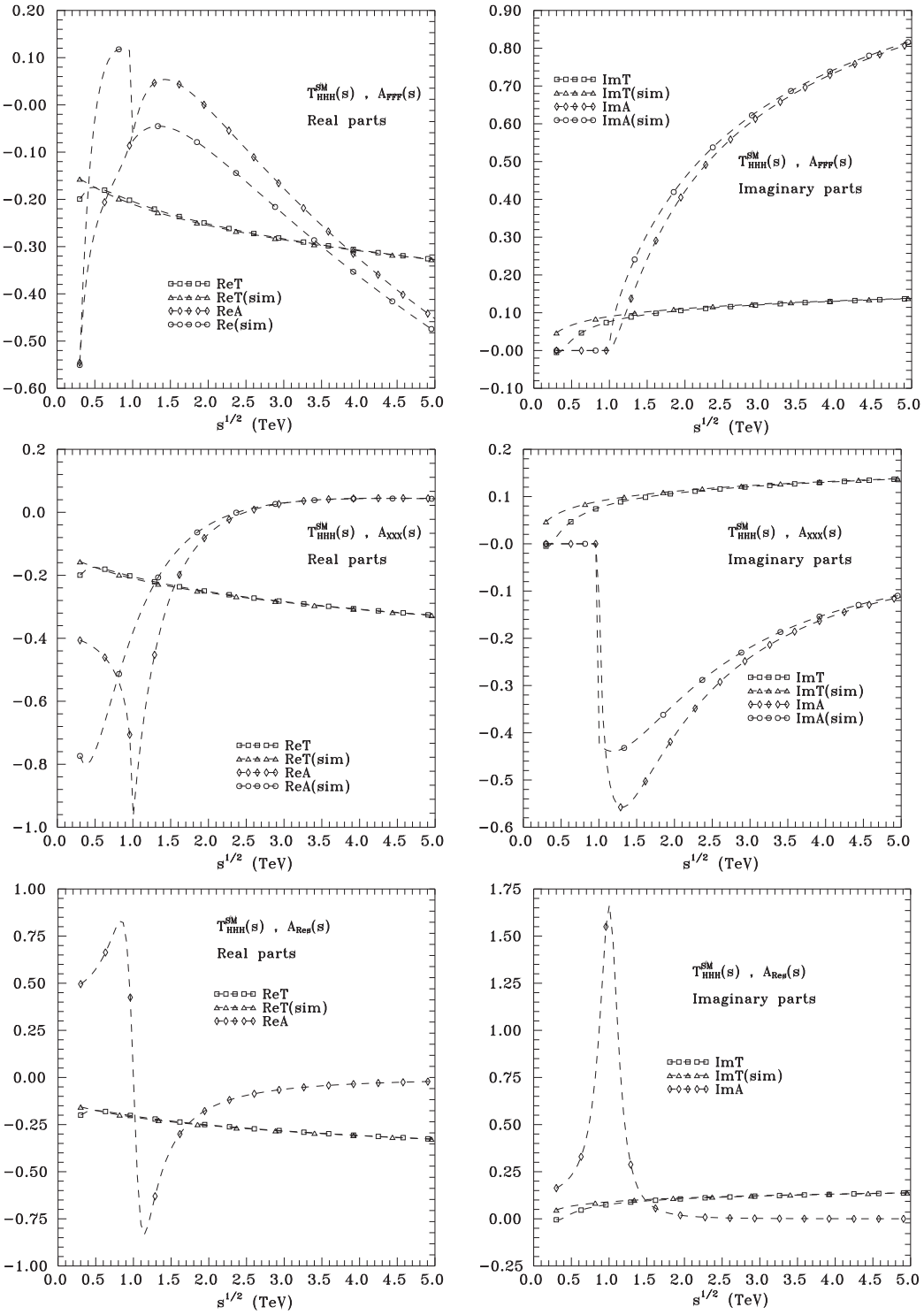

FIG. 3. The s dependence of SM form factor T^{SM}_{HHH} defined in Eq. (7), together with the new physics contributions to it from $A(s)_{FFF}$ of Eq. (21) (upper panels), $A(s)_{XXX}$ of Eq. (20) (middle panels), and $A(s)_{\mathrm{Res}}$ of Eq. (22) (lower panels). Left and right panels present real and imaginary parts, respectively. T refers to the SM contribution, and A refers to the new physics contributions, with the following parameters $m_X = 0.5$ TeV and $g_{HXX} = -10$ TeV, $m_F = 0.5$ TeV and $g_{HFF} = -4$, $M_R = 1$ TeV, $\Gamma_R = 0.3$ TeV, and $g_{HR}g_{RHH} = 0.5$ TeV. The SRS predictions given in Eqs. (A1) and (A2) are denoted T(sim).

HHH form factor. On the contrary, the HC cross section has a specific angular shape; it starts with smaller values at low energy but becomes of comparable size to the HV one at high energies, due to the large box contributions.

The unpolarized cross section contains all these features but obviously does not allow their easy disentangling.

IV. ANOMALOUS HHH CONTRIBUTIONS

We are now looking for possible effects of a modification of the SM HHH form factor due to new physics contributions. They will only affect the HV helicity amplitudes according to the H exchange diagram, giving

$$\delta F_{\lambda,\lambda'} = \frac{e g_{\mu\mu H}\delta T_{HHH}(s)}{s - m_H^2 + i m_H \Gamma_H}\sqrt{s}\,\delta_{\lambda,\lambda'}, \tag{15}$$

where $\delta T_{HHH}(s)$ is the departure to the SM prediction $T^{\rm SM}_{HHH}(s)$ in Eq. (7), which is induced by the H self-energy and HHH form factor discussed in Sec. III, item i.c.

A. Examples of new physics contributions

Our aim is not to study particular new models but only to look at the sensitivity of the $\mu^-\mu^+ \to HH$ process to modifications of the SM g_{HHH} coupling and especially to the s-dependent form factor that they generate.

Modifications are often described by effective operators; see Refs. [6,7]. There are various types of dimension-6 operators leading to anomalous couplings. Among them, we can mention the ones generating direct effective $\mu\mu HH$ couplings like

$$O = \frac{c}{\Lambda^2}(H^\dagger \overleftrightarrow{D}_\mu H)(\bar\mu\gamma^\mu P_{L,R}\mu), \tag{16}$$

which would add global contributions to the $\mu^-\mu^+ \to HH$ amplitude of the type

$$c\frac{s}{\Lambda^2}v(l',\lambda')(\not{p}' - \not{p})P_{L,R}u(l,\lambda) \tag{17}$$

as long as $s \ll \Lambda^2$, where Λ is an effective new physics scale.

More closely related to our study of the HHH form factor, there is also a dimension-6 operator,

$$O_T = \frac{c_T}{2\Lambda^2}(H^\dagger \overleftrightarrow{D}_\mu H)^2, \tag{18}$$

which would give an additional contribution $\delta T_{HHH}(s)$ to the standard HHH coupling of the type $c_T(s/\Lambda^2)$.

However, these descriptions only parametrize a departure from the SM prediction as long as $s \ll \Lambda^2$ but not a complete s dependence (the shape) of the form factor, which is our purpose.

We therefore come back to the precise structure of the HHH vertex. With the idea of compositeness, we can take as an example the hadronic structure of the $\sigma\sigma\sigma$ vertex where the σ is a $q\bar q$ bound state. This vertex can be pictured through a triangular quark loop, but it is obviously affected by nonperturbative binding interactions. With such a picture, the whole HHH coupling should then come from (XXX) triangles made by the constituents X and an effective HXX coupling related to the binding. This would generate an effective HHH vertex replacing the usual SM HHH Born term. On another hand, if the Higgs boson is

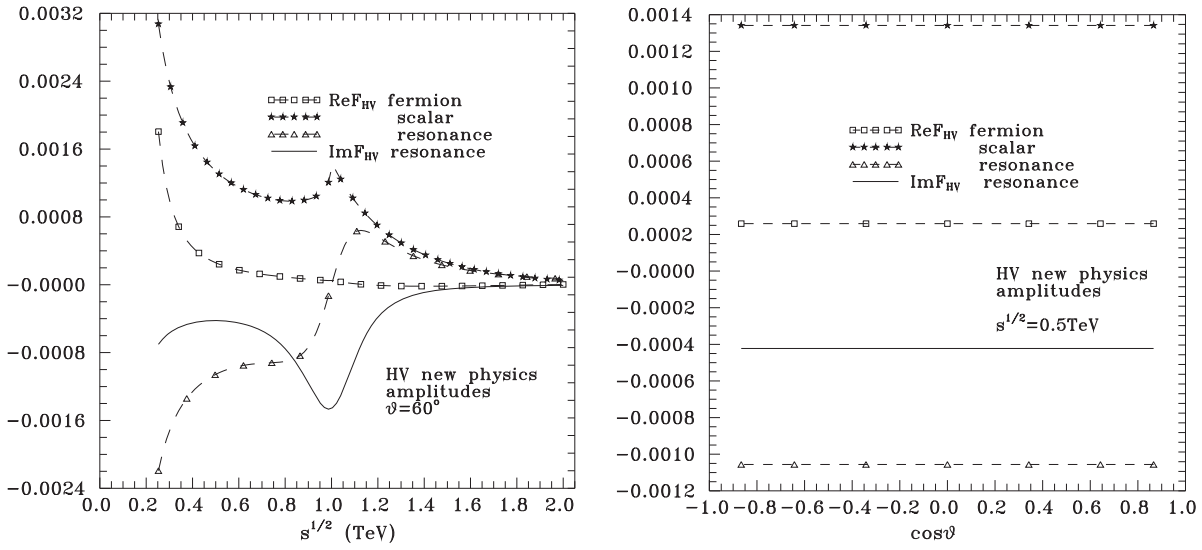

FIG. 4. The new physics contributions to the HV amplitudes induced by the HHH form factors of Fig. 3. The HC amplitudes and the imaginary parts in the "new fermion" and "new scalar" HV amplitudes are vanishing, and they are not shown. The left panel presents the energy dependencies, while the right panel presents the angular ones, as in Fig. 1.

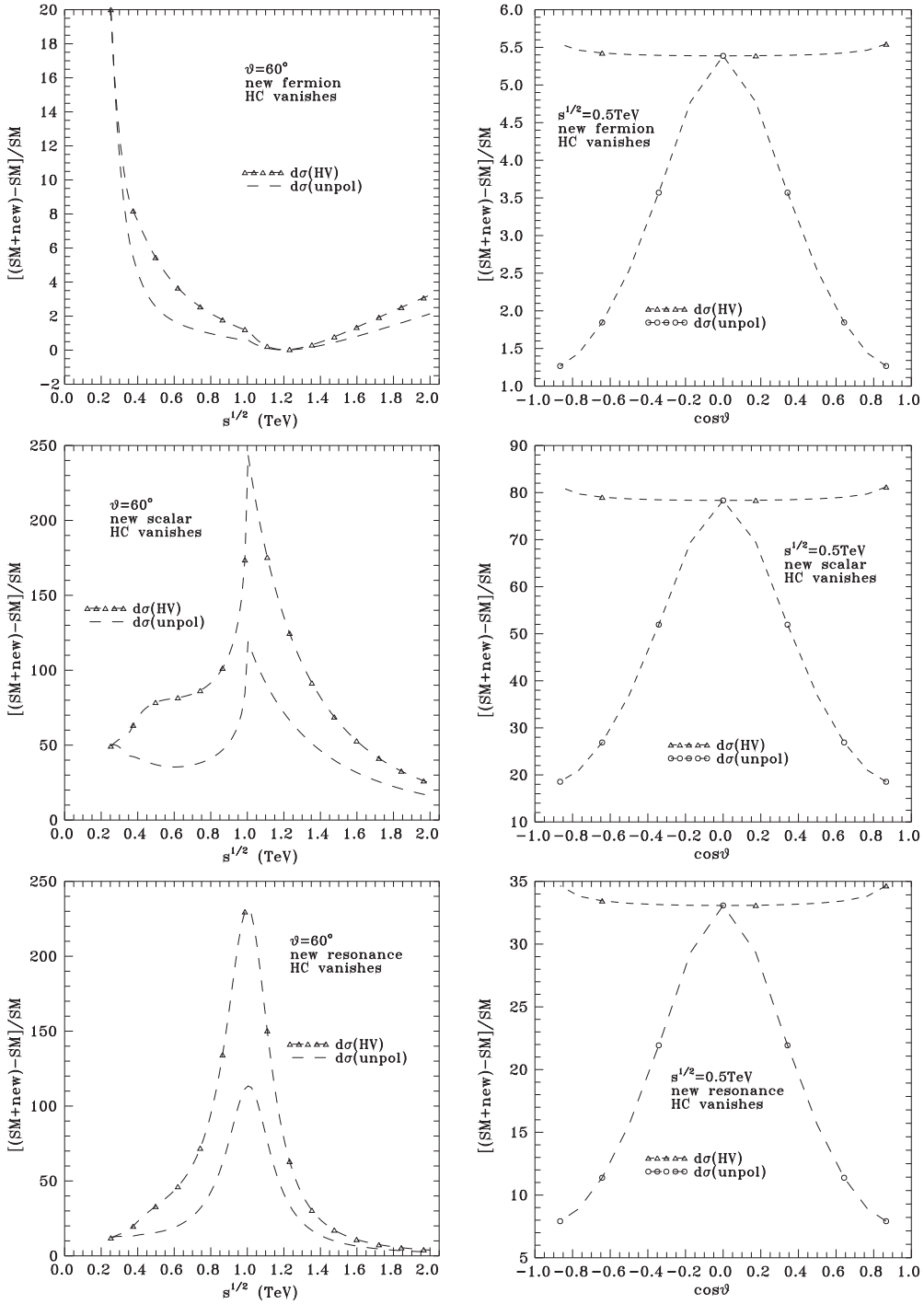

FIG. 5. Dependencies of $[d\sigma(\mathrm{SM}+\mathrm{new})/d\cos\vartheta - d\sigma(\mathrm{SM})/d\cos\vartheta]/[d\sigma(\mathrm{SM})/d\cos\vartheta]$, on the "new fermion" (upper), "new scalar" (middle), and the "new resonance" (lower panel) contributions for the total HV case in Eq. (13) and for the unpolarized case.

connected to a new sector, one may have triangles involving the corresponding new particles. In the case of a strong sector (similarly to the hadronic case), there may be resonances R leading to HHH contributions of the type $H \to R(XX) \to HH$.

In Fig. 3, we give illustrations of the contributions to the (HHH) form factor corresponding to such examples, and we compare them to the total SM one (essentially controlled by the ttt triangle) and to its super-simplicity approximation (called sim) given in Sec. III, item i.c.:

(i) For a scalar Higgs-constituent X with a g_{HXX} coupling, we get the departure $\delta T_{HHH}(s)$ due to the XXX triangle contribution to the HHH coupling,

$$\delta T_{HHH}(s) \to A_{XXX}(s) = -\frac{e\alpha}{4\pi} g_{HXX}^3 C_0(s, m_H^2, m_H^2, m_X^2, m_X^2, m_X^2), \quad (19)$$

where C_0 is the Passarino-Veltman [21] function. Using its high-energy expansion [31], one gets [see Eq. (A1)]

$$-\frac{e\alpha}{4\pi} g_{HXX}^3 \frac{\overline{\ln^2 s_X}}{2s}. \quad (20)$$

In the illustration, we take $m_X = 0.5$ TeV and $g_{HXX} = -10$ TeV.

(ii) For a fermionic constituent F, we get similarly the departure due to the FFF triangle

$$\begin{aligned}\delta T_{HHH}(s) &\to A_{FFF}(s) \\ &= -\frac{e\alpha}{4\pi} g_{HFF}^3 \{2m_F^3 C_0 + 2m_F[3m_H^2(C_{21} + C_{22}) \\ &\quad + 6p.p' C_{23} + 3nC_{24} + 2q.pC_{11} + 2q.p' C_{12} \\ &\quad + 2m_H^2 C_{11} + 2p.p' C_{12} + q.pC_0]\} \\ &\to -\frac{e\alpha}{4\pi} g_{HFF}^3 \left\{2m_F \left[\frac{-\overline{\ln^2 s_F}}{4} - \overline{\ln s_{FF}}\right]\right\}, \end{aligned} \quad (21)$$

with the notations defined in Eqs. (A1) and (A2) of the Appendix. In the illustration, we take $m_F = 0.5$ TeV and $g_{HFF} = -4$.

(iii) For a typical resonance effect, we get the (trivial) shape

$$\delta T_{HHH}(s) \to A_{\rm Res}(s) = \frac{g_{HR} g_{RHH}}{s - M_R^2 + iM_R\Gamma_R}. \quad (22)$$

The illustration is made with $M_R = 1$ TeV, $\Gamma_R = 0.3$ TeV, $g_{HR} g_{RHH} = 0.5$ TeV.

The numerical values of the above masses and effective couplings have been chosen such that, in the illustrations, the shape of the resulting HHH form factor can be quickly compared with that of the SM case such that one can appreciate the different spectacular s dependencies. One indeed sees that the s dependencies appearing in these examples are very different from each other and also very different from the SM case.

So, we believe that there is much to learn from the measurement of the HHH form factor.

We can now see how this is reflected in the HV $\mu^-\mu^+ \to HH$ amplitudes (see Fig. 4) and in the cross sections (see Fig. 5) with their specific energy dependencies, threshold effects, and resonance shapes.

In Fig. 5, we show the relative differences $[\sigma_{\rm SM+NP} - \sigma_{\rm SM}]/\sigma_{\rm SM}$ between the cross sections involving these new contributions and the pure SM cross sections, for the HV contribution [see Eq. (13)] and for the unpolarized case. Because of the common dominating final $\delta T_{HHH}(s)$ term, the left-left and right-right HV cases defined in Eq. (13) would give similar results to the complete HV case. So, one sees that polarized beams allowing the separation of HV from HC contributions would help to differentiate HHH form factor effects from possible other anomalous effects.

As one can see in the illustrations, the s and θ dependencies of the cross sections (even the unpolarized one) should allow one to identify the nature of the new contribution.

At this point, we should add a few words about the observability of such effects. The energy of a $\mu^-\mu^+$ collider has been considered up to 6 TeV [22]. For our study, the required energy would correspond to the yet unknown new physics scale, although the curious anomalies observed at the LHC around 0.75 and 2 TeV [23] could be in mind, but it is too early to know how they would affect the HHH coupling.

With an expected luminosity of the order of 10^{35} cm^{-2} s^{-1} [22], the SM cross section (see Fig. 2) would lead to only a few events per year. But we have seen that large enhancements could appear due to anomalous HHH couplings, threshold, and resonance effects in the HHH form factor, which should then be observable. In case these luminosities could not be reached, we can mention that there may be other processes (for example, WW fusion; see the next section) where HH production could be observed with a higher statistics; see, for example, Ref. [24].

V. CONCLUSIONS

In this work, we have computed the full one-loop SM contributions to the $\mu^-\mu^+ \to HH$ process, and we have studied the role of the final HHH coupling and of its SM form factor. Our aim is to show how possible new contributions to the HHH form factor could be identified through observables. We have emphasized the specific properties of the HC and HV amplitudes and their energy and angular dependencies and how this reflects in the observable polarized and unpolarized cross sections.

We have compared the real and imaginary parts of the SM one-loop contributions to the HHH form factor, to examples of possible new physics effects corresponding either to Higgs boson compositeness, or to the coupling of the Higgs boson to a new sector. In each case, we have also given the corresponding simple analytic expressions, in the adequate "sim" approximation discussed in the Appendix, allowing a quick estimate of the effect at high s.

We have emphasized the fact that the $q^2 \equiv s$ dependencies of the HHH form factor can be very different, depending on their origin. We have taken some arbitrary cases with new scalar or new fermion contributions to the HHH form factor, or strong resonances, and made the corresponding illustrations. As it can be seen in these illustrations, the differences can be spectacular and reflect the specific nature of the new physics.

We have shown that polarized cross sections ($\mu^{\mp}$ beam polarization could be available according to some studies [15,16]) are essential for differentiating HV contributions (which are the only ones containing HHH form factor effects) from HC contributions.

But even the shape of the s and θ dependencies of the unpolarized cross sections should help for identifying the nature of the new contribution.

The present study is an example of what could be done for the search of HHH form factor effects in the process $\mu^-\mu^+ \to HH$. Spectacular resonance or threshold effects could easily be seen, but high luminosity would be required in order to make precise analyses. This would correspond to the simplest situation.

More complex processes like $ZZ \to HH$, $W^-W^+ \to HH$, $gg \to HH$, or $\gamma\gamma \to HH$ could be considered and would benefit from larger cross sections at e^-e^+, $\mu^-\mu^+$ colliders or at the LHC. Note that the fusion subprocesses $ZZ \to HH$ and $W^-W^+ \to HH$ involve, like in the above $\mu^-\mu^+$ case, the simple s-channel H exchange diagram, with in addition a four-leg $ZZHH$ or W^-W^+HH vertex, as well as t- and u-channel Z or W exchanges. These subprocesses can be measured by making detailed specific analyses.

The processes $gg \to HH$ and $\gamma\gamma \to HH$ contain an s-channel H exchange, but the initial vertex needs a one-loop contribution, and there are also several other one-loop diagrams producing the final HH state. Specific works should be devoted to each of these processes; see, e.g., Refs. [25–29].

The aim of this paper was only to put forward the idea of looking especially at the s dependence of the HHH form factor and to show that observable consequences may exist.

We hope that these first results will encourage further phenomenological and experimental studies of the possibilities to measure this form factor.

APPENDIX: SM CONTRIBUTIONS TO THE HHH FORM FACTOR

The SM prediction for the HHH form factor consists of a zero-order contribution given by the pointlike coupling g_{HHH} in Eq. (3) and of higher-order corrections. In the OS scheme [18,19], these corrections consist of parameter renormalization and additional one-loop diagrams. We are interested in the $q^2 \equiv s$ dependence when one H is off shell, while the two other H (with 4-momenta p, p') are on shell, in order to make the comparison of this SM prediction with possible compositeness structures.

So, we will use a procedure allowing us to quickly get simple forms which reflect sufficiently well the size and the s dependence of each contribution. This is the SRS procedure [20,30], which leads to the simplest expressions in terms of augmented Sudakov logarithms. Among them, we will only need the augmented Sudakov forms (see Refs. [20,30] for details),

$$\overline{\ln^2 s_X} \equiv \ln^2 s_X + 4L_{HXX}, \qquad s_X \equiv \left(\frac{-s-i\epsilon}{m_X^2}\right), \tag{A1}$$

$$\overline{\ln s_{ij}} \equiv \ln s_{ij} + b_0^{ij}(m_H^2) - 2, \quad \ln s_{ij} \equiv \ln\frac{-s-i\epsilon}{m_i m_j}, \tag{A2}$$

where (X, i, j) refer to internal exchanges in the contributing diagrams. The explicit expressions for $b_0^{ij}(m_H^2)$ and L_{HXX} are given, e.g., in Eqs. (A.6) and (A.5) of Ref. [30]. We note that the counterterms needed in the SRS scheme respect the structure (A1), (A2) [20,30].

Globally, this procedure consists in replacing the divergent terms related to the (i, j) internal lines of any contributing diagram, as

$$\ln\frac{-s-i\epsilon}{\mu^2} - \Delta \to \ln s_{ij} + b_0^{ij}(m_H^2), \tag{A3}$$

where μ here denotes the renormalization scale and $\Delta = 1/\epsilon - \gamma_E + \ln(4\pi)$, with the number of dimensions used for regularization written as $n = 4 - 2\epsilon$.

In the present case, with only triangle and bubble diagrams contributing, there is no ambiguity related to the internal lines (i, j). They can only be H, Z, W, and t so that we can only have $(ij) = (HH), (ZZ), (WW), (tt)$. The SRS results thus obtained are always denoted as "sim" in the illustrations [20,30].

We next describe the exact expressions for the various triangle and bubble diagrams with four-leg couplings as well as their high-energy SRS (sim) forms. At first α order, the $T^{\rm SM}_{HHH}(s)$ form factor of Eq. (7) may be written as

$$T^{\rm SM}_{HHH}(s) = e g_{HHH} + A^{\rm SM}(s). \tag{A4}$$

In the following two subsections, we first give the $A^{\rm SM}(s)$ results implied by the one-loop triangles and bubbles with four-leg couplings and then from the H self-energy.

1. Triangles and bubbles with four-leg couplings

Depending on the natures of the exchanged particles, the contributions to $A^{\rm SM}(s)$ from the various two-point and three-point Passarino-Veltman functions, denoted as B and C, are given by [21,31]

(i) Scalar (SSS) triangles and (SS) bubbles with a 4-leg $SSHH$ coupling:

$$\begin{aligned} A^{\rm SM}_{SSS}(s) = &-\frac{e\alpha}{4\pi}\{g^3_{HSS} C_0(s, m_H^2, m_H^2, m_S^2, m_S^2, m_S^2) \\ &+ g_{HSS} g_{HHSS}[B_0(s, m_S^2, m_S^2) \\ &+ 2B_0(m_H^2, m_S^2, m_S^2]\} \\ \to &-\frac{e\alpha}{4\pi}\left\{g^3_{HSS}\frac{\overline{\ln^2 s_S}}{s} - g_{HSS} g_{HHSS}\overline{\ln s_{SS}}\right\}. \end{aligned} \tag{A5}$$

This applies to the triangles

$$SSS = HHH, G^0G^0G^0, C^ZC^ZC^Z, G^\pm G^\pm G^\pm, C^\pm C^\pm C^\pm$$

and the bubbles

$$SS = HH, G^0G^0, G^\pm G^\pm,$$

while g_{HHH} is given in Eq. (3) and[2]

$$g_{HHHH} = -\frac{3m_H^2}{4s_W^2 m_W^2}, \qquad g_{HGG} = -\frac{m_H^2}{2s_W m_W},$$
$$g_{HHGG} = \frac{1}{2s_W^2 c_W^2},$$
$$g_{HC^ZC^Z} = -\frac{m_W}{2s_W c_W^2}, \qquad g_{HC^\pm C^\pm} = -\frac{m_W}{2s_W}. \quad \text{(A6)}$$

Note that there is no four-leg diagram for the ghost loop and that a global fermionic minus sign has been inserted. In all cases, the internal S mass for $H, G^0, C^Z, G^\pm, C^\pm$ is respectively equal to the one of H, Z, Z, W, W.

(ii) Fermion triangles (fff): Because of the strong mass dependence of the Hff coupling, it is adequate to restrict to the $(ttt) + (\bar{t}\bar{t}\bar{t})$ case. The result is

$$A_{ttt}^{\rm SM}(s) = \frac{e\alpha}{4\pi}\frac{3m_t^3}{2s_W^3 m_W^3}\{2m_t^3 C_0 + 2m_t[3m_H^2(C_{21}+C_{22}) + 6p.p'C_{23} + 3nC_{24} + 2q.pC_{11} + 2q.p'C_{12} + 2m_H^2 C_{11} + 2p.p'C_{12} + q.pC_0]\} \to \frac{e\alpha}{4\pi}\frac{3m_t^3}{2s_W^3 m_W^3}\left\{2m_t\left[\frac{-\overline{\ln^2 s_t}}{4} - \overline{\ln s_{tt}}\right]\right\}. \quad \text{(A7)}$$

(iii) Vector triangles (VVV) and bubbles (VV) with a four-leg $HHVV$ coupling:

$$A_{VVV}^{\rm SM}(s) = \frac{e\alpha}{4\pi}\{g_{HVV}^3 nC_0 + g_{HVV}g_{HHVV}[2B_0(m_H^2, m_V^2, m_V^2) + B_0(s, m_V^2, m_V^2)]\} \to -\frac{e\alpha}{4\pi}\left\{2g_{HVV}^3\frac{\overline{\ln^2 s_V}}{s} + g_{HVV}g_{HHVV}[-\overline{\ln s_{VV}}]\right\}, \quad \text{(A8)}$$

applied only to $V = Z, W$, since there are no $HZ\gamma$ or $HHZ\gamma$ couplings. Because of this, the V masses in the SRS forms $\overline{\ln^2 s_V}$ and $\overline{\ln s_{VV}}$ can either be m_Z or m_W.

(iv) (VVS) triangles:

$$A_{VVS}^{\rm SM}(s) = \frac{e\alpha}{4\pi}g_{VSH}^2 g_{VVH}^2\{m_H^2(C_{21}+C_{22}) + 2p.p'C_{23} + nC_{24} + (p.p'+3q.p)C_{11} + (m_H^2 + 3q.p')C_{12} + 2(q^2 + q.p')C_0\} \to \frac{e\alpha}{4\pi}g_{VSH}^2 g_{VVH}^2\left\{\frac{1}{2}(\overline{\ln^2 s_V} + \overline{\ln s_{VV}})\right\}, \quad \text{(A9)}$$

applied to $ZZG^0, W^\pm W^\pm G^\pm$; compare Eq. (A8).

(v) (VSV) triangles:

$$A_{VSV}^{\rm SM}(s) = \frac{e\alpha}{4\pi}g_{VSH}^2 g_{VVH}^2\{m_H^2(C_{21}+C_{22}) + 2p.p'C_{23} + nC_{24} + (3m_H^2 - p.p')(C_{11} - C_{12}) + 2(m_H^2 - p.p')C_0\} \to \frac{e\alpha}{4\pi}g_{VSH}^2 g_{VVH}^2\left\{\frac{1}{4}\overline{\ln^2 s_V} + 2\overline{\ln s_{VV}}\right\}, \quad \text{(A10)}$$

applied to $ZG^0Z, W^\pm G^\pm W^\pm$.

(vi) (SVV) triangles:

$$A_{SVV}^{\rm SM}(s) = \frac{e\alpha}{4\pi}g_{VSH}^2 g_{VVH}^2\{m_H^2(C_{21}+C_{22}) + 2p.p'C_{23} + nC_{24} - (m_H^2 + q.p)C_{11} - (p.p' + q.p')C_{12}) + q.pC_0\} \to \frac{e\alpha}{4\pi}g_{VSH}^2 g_{VVH}^2\left\{-\frac{1}{2}(\overline{\ln^2 s_V} + \overline{\ln s_{VV}})\right\}, \quad \text{(A11)}$$

applied to $G^0ZZ, G^\pm W^\pm W^\pm$.

(vii) (VSS) triangles:

$$A_{VSS}^{\rm SM}(s) = \frac{e\alpha}{4\pi}g_{VSH}^2 g_{SSH}^2\{-m_H^2(C_{21}+C_{22}) - 2p.p'C_{23} - nC_{24} - 2(m_H^2 + q.p)C_{11} - 2(p.p' + q.p')C_{12}) - 4q.pC_0\} \to \frac{e\alpha}{4\pi}g_{VSH}^2 g_{SSH}^2\left\{-\frac{1}{2}\overline{\ln^2 s_V} + \overline{\ln s_{VV}}\right\}, \quad \text{(A12)}$$

applied to $ZG^0G^0, W^\pm G^\pm G^\pm$.

[2] $(G^\pm, G^0)$ denote the SM Goldstone fields, and $(C^\pm, C^Z)$ denote the Faddeev-Popov (FP) ghosts.

(viii) (SVS) triangles:

$$\begin{aligned}A^{\rm SM}_{SVS}(s)=&\frac{e\alpha}{4\pi}g^2_{VSH}g^2_{SSH}\{-m_H^2(C_{21}+C_{22})-2p.p'C_{23}\\&-nC_{24}-(-m_H^2+q.p+p.p')C_{11}\\&-(m_H^2-p.p'+q.p')C_{12})\\&+(p.p'+q.p)C_0\}\\&\to\frac{e\alpha}{4\pi}g^2_{VSH}g^2_{SSH}\{\overline{\ln^2 s_V}-\overline{\ln s_{VV}}\},\end{aligned}\tag{A13}$$

applied to $G^0ZG^0, G^\pm W^\pm G^\pm$.

(ix) (SSV) triangles:

$$\begin{aligned}A^{\rm SM}_{SSV}(s)=&\frac{e\alpha}{4\pi}g^2_{VSH}g^2_{SSH}\{-m_H^2(C_{21}+C_{22})-2p.p'C_{23}\\&-nC_{24}-(m_H^2-q.p-p.p')C_{11}\\&-(-m_H^2+p.p'-q.p')C_{12})\\&+(-q.p'+q.p)C_0\}\\&\to\frac{e\alpha}{4\pi}g^2_{VSH}g^2_{SSH}\left\{-\frac{1}{2}\overline{\ln^2 s_V}+\overline{\ln s_{VV}}\right\},\end{aligned}\tag{A14}$$

applied to $G^0G^0Z, G^\pm G^\pm W^\pm$.

In the above contributions, the following couplings are needed:

$$\begin{aligned}g_{ZZH}&=\frac{m_Z}{s_Wc_W},\qquad g_{ZZHH}=\frac{1}{2s_W^2c_W^2},\\g_{WWH}&=\frac{m_W}{s_W},\qquad g_{WWHH}=\frac{1}{2s_W^2},\\g_{ZGH}&=g_{WGH}=\frac{1}{2s_Wc_W}.\end{aligned}\tag{A15}$$

2. H self-energy

This additional contribution is given by

$$A^{\rm SM}_{se}(s)=-\frac{eg_{HHH}}{s-m_H^2}\Sigma_H(s),\tag{A16}$$

where $\Sigma_H(s)$ is computed from the following diagrams:

(i) Bubbles VV leading to

$$\Sigma_H(s)=\frac{X_1^2}{4\pi^2}[B_0]\to\frac{X_1^2}{4\pi^2}[-\overline{\ln s_{VV}}],\tag{A17}$$

for which we respectively get

$$\begin{aligned}VV=ZZ\to X_1^2&=\frac{e^2M_W^2}{2s_W^2c_W^4},\\VV=W^\pm W^\mp\to X_1^2&=\frac{e^2M_W^2}{s_W^2}.\end{aligned}\tag{A18}$$

(ii) Bubbles SV leading to

$$\begin{aligned}\Sigma_H(s)&=-\frac{X_1^2}{16\pi^2}[s(B_0+B_{21}-2B_1)+nB_{22}]\\&\to-\frac{X_1^2}{16\pi^2}[-2s\overline{\ln s_{SV}}],\end{aligned}\tag{A19}$$

for which we respectively get

$$\begin{aligned}SV=G^0Z\to X_1^2&=\frac{e^2}{4s_W^2c_W^2},\\SV=G^\mp W^\pm\to X_1^2&=\frac{e^2}{2s_W^2}.\end{aligned}\tag{A20}$$

(iii) Bubble tt leading to

$$\begin{aligned}\Sigma_H(s)&=-\frac{1}{4\pi^2}[(s(B_1+B_{21})+nB_{22}+m_t^2B_0)X_1^2]\\&\to-\frac{X_1^2}{4\pi^2}\left[\frac{s}{2}\overline{\ln s_{tt}}\right],\end{aligned}\tag{A21}$$

with

$$X_1^2=\frac{3e^2}{4s_W^2M_W^2}[m_t^2].\tag{A22}$$

(iv) Bubbles SS leading to

$$\Sigma_H(s)=\frac{X_1^2}{16\pi^2}[B_0]\to\frac{X_1^2}{16\pi^2}[-\overline{\ln s_{SS}}],\tag{A23}$$

with

$$\begin{aligned}X_1^2=&\frac{9e^2m_H^4}{8s_W^2M_W^2},\qquad\frac{e^2m_H^4}{8s_W^2M_W^2},\qquad\frac{e^2m_H^4}{4s_W^2M_W^2},\\&-\frac{e^2m_W^2}{4s_W^2c_W^4},\qquad-\frac{e^2m_W^2}{2s_W^2},\end{aligned}\tag{A24}$$

for

$$SS=HH, G^0G^0, G^+, G^-, C^ZC^Z, C^+C^-,\tag{A25}$$

respectively. Note that in these SS bubbles the internal S mass is correspondingly equal to the mass of H, Z, W, Z, W.

[1] G. Aad *et al.* (ATLAS Collaboration), Phys. Lett. B **716**, 1 (2012); S. Chatrchyan *et al.* (CMS Collaboration), Phys. Lett. B **716**, 30 (2012); G. J. Davies (CDF and D0 Collaborations), Front. Phys. **8**, 270 (2013); ATLAS Collaboration, https://twiki.cern.ch/twiki/bin/view/AtlasPublic/HiggsPublicResults;CMS Collaboration, https://twiki.cern.ch/twiki/bin/view/CMSPublic/PhysicsResultsHIG.
[2] P. Higgs, Phys. Lett. **12**, 132 (1964); Phys. Rev. Lett. **13**, 508 (1964); Phys. Rev. **145**, 1156 (1966); F. Englert and R. Brout, Phys. Rev. Lett. **13**, 321 (1964); G. Guralnik, C. Hagen, and T. Kibble, Phys. Rev. Lett. **13**, 585 (1964).
[3] S. L. Glashow, Nucl. Phys. **B22**, 579 (1961); S. Weinberg, Phys. Rev. Lett. **19**, 1264 (1967); A. Salam, *Proceedings of the 8th Nobel Symposium*, edited by N. Svartholm (Almqvist and Wiskell, Stockholm, 1968), p. 367.
[4] B. Gripaios, arXiv:1503.02636; arXiv:1506.05039; A. Wulzer, *Proc. Sci.*, EPS-HEP2015, (2015) 005.
[5] See A. Djouadi, Phys. Rep. **457**, 1 (2008) and arXiv:1505.01059.
[6] G. F. Giudice, C. Grojean, A. Pomarol, and R. Rattazzi, J. High Energy Phys. 06 (2007) 045.
[7] J. Ellis, V. Sanz, and T. You, J. High Energy Phys. 03 (2015) 157.
[8] B. Patt and F. Wilczek, arXiv:hep-ph/0605188.
[9] H. Terazawa, Y. Chikashige, and K. Akama, Phys. Rev. D **15**, 480 (1977); for other references, see H. Terazawa and M. Yasue, arXiv:1508.00172; J. Mod. Phys. **05**, 205 (2014).
[10] D. B. Kaplan and H. Georgi, Phys. Lett. **136B**, 183 (1984); K. Agashe, R. Contino, and A. Pomarol, Nucl. Phys. **B719**, 165 (2005).
[11] R. Contino, T. Kramer, M. Son, and R. Sundrum, J. High Energy Phys. 07 (2005) 076.
[12] G. Panico and A. Wulzer, Lect. Notes Phys. **913**, 1 (2016).
[13] M. E. Peskin, arXiv:1506.08185; M. Muhlleitner, arXiv:1410.5093.
[14] J. Baglio *et al.*, arXiv:1212.5581; J. High Energy Phys. 04 (2013) 151.
[15] D. B. Cline, Nucl. Instrum. Methods Phys. Res., Sect. A **350** (1994) 24; V. D. Barger, M. S. Berger, J. F. Gunion, and T. Han, Phys. Rep. **286**, 1 (1997); C. Rubbia, arXiv:1308.6612; Y. Alexahin *et al.*, arXiv:1308.2143; D. Neuffer *et al.*, arXiv:1502.02042.
[16] D. Cline *et al.*, acc-phys/9609002; B. Grzadkowski *et al.*, arXiv:hep-ph/0003091.
[17] G. J. Gounaris and F. M. Renard, Phys. Rev. Lett. **94**, 131601 (2005); Phys. Rev. D **73**, 097301 (2006).
[18] M. Böhm, H. Spiesberger, and W. Hollik, Fortschr. Phys. **34**, 687 (1986); W. Hollik, Fortschr. Phys. **38**, 165 (1990); A. Denner, Fortschr. Phys. **41**, 307 (1993).
[19] A. Dobado, M. J. Herrero, W. Hollik, and S. Peñaranda, Phys. Rev. D **66**, 095016 (2002).
[20] G. J. Gounaris and F. M. Renard, Acta Phys. Pol. A **42**, 2107 (2011); Phys. Rev. D **86**, 013003 (2012); **90**, 073007 (2014).
[21] G. Passarino and M. Veltman, Nucl. Phys. **B160**, 151 (1979).
[22] J. P. Delahaye *et al.*, arXiv:1502.01647.
[23] ATLAS note, ATLAS-Conf-2015-081; CMS note, CMS PAS EXO-15-004.
[24] A. Conway, H. Wentzel, E. Eichten, and R. Lipton, arXiv:1405.5910.
[25] R. Contino, M. Ghezzi, M. Moretti, G. Panico, F. Piccinini, and A. Wulzer, J. High Energy Phys. 08 (2012) 154; C.-R. Chen and I. Low, Phys. Rev. D **90**, 013018 (201); F. Goertz, A. Papaefstathiou, L. L. Yang, and J. Zurita J. High Energy Phys. 04 (2015) 167; A. Azatov, R. Contino, G. Panico, and M. Son, Phys. Rev. D **92**, 035001 (2015).
[26] S. Dawson, A. Ismail, and I. Low, Phys. Rev. D **91**, 115008 (2015).
[27] V. I. Telnov, J. Instrum. **9**, C09020 (2014).
[28] E. Asakawa *et al.*, arXiv:1009.4670; Phys. Rev. D **82**, 115002 (2010).
[29] A. Levy, Eur. Phys. J. Web Conf. **95**, 03022 (2015).
[30] G. J. Gounaris and F. M. Renard, Phys. Rev. D **88**, 113003 (2013).
[31] M. Beccaria, G. J. Gounaris, J. Layssac, and F. M. Renard, Int. J. Mod. Phys. A **23**, 1839 (2008).